Ocean Engineering 144 (2017) 1–13

Contents lists available at ScienceDirect

Ocean Engineering

journal homepage: www.elsevier.com/locate/oceaneng

Study on added resistance of a ship under parametric roll motion

Jae-Hoon Lee, Yonghwan Kim*

Department of Naval Architecture and Ocean Engineering, Seoul National University, Republic of Korea

ARTICLE INFO

Keywords:
Parametric roll
Nonlinear roll
Added resistance
Rankine panel method
Ship stability

ABSTRACT

Parametric roll of ship is a rare event occurring in specific conditions, but it can cause the dynamic roll instability. Since this phenomenon is dependent on ship speed and wave frequency, the development of roll motion and the resultant added resistance which can cause speed change should be considered simultaneously when parametric roll occurs. This paper considers a numerical study on the added resistance of a modern containership under parametric roll. A time-domain Rankine panel method adopting a weakly nonlinear formulation is adopted to obtain ship motions and added resistances in waves. Seakeeping computations in regular head-sea conditions are performed with and without parametric roll, and the increment of added resistance is investigated with regard to the components classified in the direct pressure integration method. Furthermore, according to the decoupling phenomena between the components of the vertical motions and the roll motion, a correlation between the parametric roll and the added resistance is derived. Lastly, a simple prediction method for the added resistance in irregular parametric roll motion is suggested based on the correlation, and its accuracy and efficiency are discussed by comparing the prediction with the results of the direct numerical computation.

1. Introduction

Prevention of the parametric roll phenomena, which is one of the dynamic stability problems of ships, has been a matter of concern, because the resonant roll motion is excited rapidly during several encounter periods of waves. Although there have been attempts to examine a direct control on the roll motion, such as the application of the bilge keel and the active fin stabilizer (Levadou and van't Veer, 2011), and the U-tank (Holden, 2011), the operational guidance for a ship crew's decision-support system can serve as a prior counter-measure in order to avoid vulnerable environmental and operational conditions to the phenomena (Song et al., 2013). The conditions are directly related to the encounter wave frequency; therefore, the forward speed and the heading angle of ships should be controlled for its prevention.

When the excitation of parametric roll starts under the vulnerable conditions, the speed of ship is changed simultaneously due to the added resistance occurred in the phenomena. Therefore, in order to tackle vulnerabilities relevant to the parametric roll, the speed variations should be accounted in numerical simulations. To this end, the accurate prediction of the added resistance induced by the large-amplitude roll motion is also required. In other words, with regard to the parametric roll phenomena, the added resistance of a ship is considered in terms of the dynamic stability in waves, not the efficiency during ship operations.

Historically, the added resistance due to waves has been widely investigated because the actual performance of ships in seaways is determined by the resistance. Several previous researchers conducted experiments for the added resistances on the typical ship models such as the series 60 models (Gerritsma and Beukelman, 1972), the S175 containership (Fujii and Takahashi, 1975), and the Wigley models (Journee, 1992). In the cases of analytical and numerical approaches, two major methods have been introduced to analyze the added resistance problem. First, a far-field method, which was originally derived by Maruo (1960) and further refined by Newman (1967), is based on a momentum conservation theory. This method is simple and efficient that does not involve solving a boundary value problem for the pressure acting on a body. In the method, however, there are difficulties in handling a proper control surface. Alternatively, a near-field method, which represents direct integration of the second-order pressure on the body surface has also applied to the calculation of added resistance. One of the advantages of the near-field method is the decomposition of added resistance, which enables the physical observation by a component analysis and an extension to considerations for nonlinearities in the phenomenon. Faltinsen et al. (1980) validated the computation results obtained by the near-field method, and formulated a simplified asymptotic approach to enhance the results for short waves. Grue and Biberg (1993) also adopted the method along

* Corresponding author.
E-mail address: yhwankim@snu.ac.kr (Y. Kim).

http://dx.doi.org/10.1016/j.oceaneng.2017.08.015
Received 31 May 2017; Received in revised form 27 July 2017; Accepted 11 August 2017

with the frequency-domain wave Green function to evaluate the resistance induced by waves on a floating body advancing with a small speed. It should be noted that most of the researches in the early stages were based on the linear potential theories; hence, the effects of nonlinear free surface flows and hull geometries were not included.

Recently, nonlinear approaches using computational fluid dynamics (CFD) simulation have been applied owing to the development of computing power. A simulation method called the WISDAM-X was used by Orihara and Miyata (2003) and Orihara et al. (2008) to examine the added resistance for different bow shapes above the mean-water level. In this method, the Reynolds-averaged Navier-Stokes equation (RANSE) was solved using a finite volume method (FVM) in an overlapping grid system. Furthermore, Yang (2015) developed a Cartesian-grid-based method for solving the Euler equation, and investigated the effects of the nonlinear bow waves on the added resistances for different wave amplitudes. In the operation of a large modern ship, the major issues are not only the efficiency of reducing greenhouse gas emissions, but also the performance of ships in rough seas. Therefore, the trend of adopting the nonlinear simulation is expected to continue. However, there have been limitations in the application of the CFD methods, because of high computational costs and a strong dependency on the grid system.

In the case of parametric roll phenomena, the time-domain simulations for nonlinear ship motions have been conducted. The most important parameter in the numerical simulation is an accurate prediction of the time-varying nonlinear restoring forces in waves. For an efficient computation, a weakly nonlinear approach, which considers the partial nonlinearities of hull geometry, was used in many previous research efforts. For example, France et al. (2003) and Shin et al. (2004) applied the Rankine panel method (RPM) to evaluate not only the susceptibility criteria but also the amplitude of roll motion for large containerships. Spanos and Papanikolaou (2007) analyzed the parametric roll of a fishing vessel in regular waves using the impulse response function (IRF) method. Kim and Kim (2011b) developed a multi-level analysis, which include level-by-level applications of an analytical formula based on the metacentric height (GM) variation, the IRF method, and the Rankine panel method to compare the properties of each method.

For realistic simulations of parametric roll motions, the speed variation due to resistance caused by severe roll motion should be considered along with occurrences and magnitudes of the phenomena. Therefore, there have been attempts to develop the surge-roll coupled model to account for the interaction between the development of parametric roll and the speed variation (Vidic-Perunovic and Jensen, 2009). Also, Breu and Fossen (2010) applied the speed and heading control to the coupled model for mitigation of the phenomena. However, in most of the previous studies, a relatively simple method was applied to estimate the added resistance, considering only for the surge added mass and Froude-Krylov and restoring forces. On the other hand, to predict the added resistance induced by parametric roll more accurately, Lu et al. (2015) adopted a roll motion obtained by model experiments to a revised formula from the linear far-field method of Maruo (1960). However, according to a linear perspective, the method did not consider the nonlinear effects of the large-amplitude roll motion. Therefore, an efficient nonlinear approach is required to account for the effects on the added resistance.

In the present study, the time-domain 3-D Rankine panel method developed by Kim et al. (2011) is applied to predict ship motions and added resistance of a containership under the parametric roll phenomena. The near-field method derived by Joncquez (2009) and Kim and Kim (2011a), which is the direct pressure integration method for the evaluation of added resistance, is modified based on a weakly nonlinear approach. In other words, the higher-order restoring and Froude-Krylov forces at the actual wetted surface are included to consider the nonlinear effects induced by parametric roll motion. Through the decomposition analysis according to components of the near-field method, the increased resistance due to the parametric roll in a regular wave is investigated. Also, the correlation between the parametric roll motion and the added resistance is derived based on the decoupling phenomena between the components of vertical motions (heave and pitch motions) and roll motion, and the limitations of the relationship are also confirmed by considering the weakly nonlinear coupling in large-amplitude ship motions. Ultimately, a simple prediction method for the added resistance in irregular parametric roll is suggested based on the correlation, and its accuracy and efficiency are discussed in comparison with the result of the direct time-domain simulations.

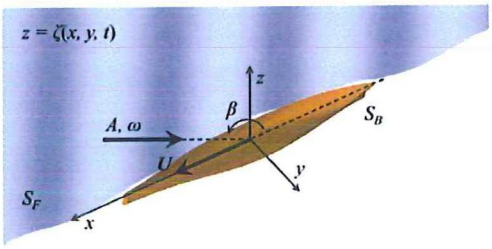

Fig. 1. Coordinate system and notations in Rankine panel method.

2. Mathematical background

2.1. Boundary value problem: Rankine panel method

Ship motions can be defined in a mean-body fixed coordinate considering a ship's advancement with a forward speed, U in waves as shown in Fig. 1. Here, A, ω, and β are the wave amplitude, frequency, and heading angle, respectively. In addition, the problem domains, S_B and S_F, denote the body surface and the free surface, respectively. When a ship is assumed to be a rigid body, it has six degrees of freedom (DOF) with the translation, $\vec{\xi}_T = (\xi_1, \xi_2, \xi_3)$, and the rotation, $\vec{\xi}_R = (\xi_4, \xi_5, \xi_6)$; the linear displacement induced by waves can be written as follows:

$$\vec{\delta}(\vec{x}, t) = \vec{\xi}_T(t) + \vec{\xi}_R(t) \times \vec{x}. \tag{1}$$

The linear potential theory is applied to the ship motions analysis. Under the assumption of an incompressible and inviscid fluid with irrotational motion, the velocity potential, ϕ satisfies the following boundary value problem:

$$\nabla^2\phi = 0 \quad \text{in fluid domain} \tag{2}$$

$$\frac{\partial\phi}{\partial n} = \vec{U}\cdot\vec{n} + \frac{\partial\vec{\delta}}{\partial t}\cdot\vec{n} \quad \text{on } S_B \tag{3}$$

$$\left[\frac{d}{dt} + \nabla\phi\cdot\nabla\right][z - \zeta(x, y, t)] = 0 \quad \text{on } z = \zeta(x, y, t) \tag{4}$$

$$\frac{d\phi}{dt} = -g\zeta - \frac{1}{2}\nabla\phi\cdot\nabla\phi \quad \text{on } z = \zeta(x, y, t) \tag{5}$$

where $d/dt = \partial/\partial t - \vec{U}\cdot\nabla$ and $\vec{U} = (U, 0, 0)$. In addition, ζ and g indicate the wave elevation and the gravitational acceleration, respectively. In this study, the total velocity potential and the wave elevation are decomposed as follows:

$$\phi(\vec{x}, t) = \Phi(\vec{x}) + \phi_I(\vec{x}, t) + \phi_d(\vec{x}, t) \tag{6}$$

$$\zeta(\vec{x}, t) = \zeta_I(\vec{x}, t) + \zeta_d(\vec{x}, t) \tag{7}$$

where Φ is the basis potential which has the order of $O(1)$. ϕ_I and ζ_I are the velocity potential and elevation of incident wave, respectively. Similarly, ϕ_d and ζ_d are those of disturbed wave, respectively. The orders of incident and disturbed components are $O(\varepsilon)$. By substitutions of Eqs. (6) and (7) into Eqs. (3)–(5), the linearized boundary conditions can be derived according to the double-body (DB) linearization,

such that:

$$\begin{aligned}
\frac{\partial \phi_d}{\partial n} &= \sum_{j=1}^{6}\left(\frac{\partial \xi_j}{\partial t}n_j + \xi_j m_j\right) - \frac{\partial \phi_I}{\partial n} \quad \text{on } \overline{S}_B \\
(n_1, n_2, n_3) &= \vec{n} \\
(n_4, n_5, n_6) &= \vec{x} \times \vec{n} \\
(m_1, m_2, m_3) &= (\vec{n}\cdot\nabla)(\vec{U} - \nabla\Phi) \\
(m_4, m_5, m_6) &= (\vec{n}\cdot\nabla)(\vec{x} \times (\vec{U} - \nabla\Phi))
\end{aligned} \tag{8}$$

$$\frac{\partial \zeta_d}{\partial t} - (\vec{U} - \nabla\Phi)\cdot\nabla\zeta_d = \frac{\partial^2 \Phi}{\partial z^2}\zeta_d + \frac{\partial \phi_d}{\partial z} + (\vec{U} - \nabla\Phi)\cdot\nabla\zeta_I \qquad \text{on } z = 0 \tag{9}$$

$$\begin{aligned}
\frac{\partial \phi_d}{\partial t} - (\vec{U} - \nabla\Phi)\cdot\nabla\phi_d = &-\frac{\partial \Phi}{\partial t} - g\zeta_d + \left[\vec{U}\cdot\nabla\Phi - \frac{1}{2}\nabla\Phi\cdot\nabla\Phi\right] \\
&+ (\vec{U} - \nabla\Phi)\cdot\nabla\phi_I \qquad \text{on } z = 0
\end{aligned} \tag{10}$$

where $\overline{S}_B$ is the surface of the mean body, and m_j denotes the m-terms, which include the coupling effects between the steady and unsteady solutions in the forward-speed ship motions problem. Furthermore, to satisfy the radiation condition, an artificial damping zone is adopted around the truncated free surface boundary. To this end, the kinematic free surface boundary condition is modified according to the artificial wave-absorbing mechanism, such that:

$$\left(\frac{\partial}{\partial t} - \vec{U}\cdot\nabla\right)\zeta_d = \frac{\partial \phi_d}{\partial z} - 2\nu\zeta_d + \frac{\nu^2}{g}\phi_d \quad \text{on } z = 0 \tag{11}$$

where ν is the damping strength, which is expressed as a quadratic form with respect to the distance from the starting point of the zone to the end of the boundary, because the strength increases gradually toward the outer domain.

To solve the derived linear boundary value problem, Green's second identity is applied as follows

$$\phi_d + \iint_{S_B}\phi_d\frac{\partial G}{\partial n}dS - \iint_{S_F}\frac{\partial \phi_d}{\partial n}GdS = \iint_{S_B}G\frac{\partial \phi_d}{\partial n}dS - \iint_{S_F}\phi_d\frac{\partial G}{\partial n}dS. \tag{12}$$

The Rankine source ($G = 1/r$), which satisfies the Laplace equation of Eq. (2), is distributed to the discretized boundary surfaces. As a result, the resulting integral equation is converted to an algebraic equation for unknown coefficients of physical variables. In the present study, the variables such as the velocity potential, the wave elevation, and their normal fluxes at the boundaries are approximated using a B-spline basis function. Furthermore, through the solutions of the algebraic equation, the instantaneous wave elevation and the velocity potential at the free surface are computed for Eqs. (9) and (10), respectively, by the time integration method such as a mixed explicit-implicit scheme. Ultimately, the hydrodynamic force due to the disturbed waves is obtained by direct integration of the pressure on the mean-body surface. The details of the numerical implementations of this 3-D Rankine panel method in time-domain can be found in Kim et al. (2011).

2.2. Equation of motion: weakly nonlinear approach

The equation of motion can be defined for the weakly nonlinear ship motion as follows:

$$[M]\{\ddot{\xi}\} = \{F_{\text{F.K.}}\}_{\text{Non.}} + \{F_{\text{Res.}}\}_{\text{Non.}} + \{F_{\text{H.D.}}\} + \{F_{\text{viscous}}\} \tag{13}$$

where $[M]$ is the mass matrix of a ship. $\{F_{\text{F.K.}}\}_{\text{Non.}}$ and $\{F_{\text{Res.}}\}_{\text{Non.}}$ indicate the nonlinear Froude-Krylov and restoring forces, respectively. In addition, $\{F_{\text{H.D.}}\}$ and $\{F_{\text{viscous}}\}$ denote the hydrodynamic force due to waves and the viscous damping force, such as a roll damping, respectively. In the weakly nonlinear approach, the hydrodynamic force is obtained according to the linear boundary conditions, while the nonlinear Froude-Krylov and restoring forces are evaluated at the actual wetted surfaces of the ship in time-domain. In other words, the partial nonlinearity induced by the hull geometry is considered in this approach, which is also known as a "blended method" between linear and nonlinear methods (Jensen et al., 2000). Therefore, the nonlinear problem, such as the parametric roll phenomena, where the prediction for the nonlinear restoring force is important can be tackled efficiently without a fully nonlinear computation.

The nonlinear Froude-Krylov forces are computed through the velocity potential of an incident wave below the mean-water level, while the first-order perturbed potential with respect to the wave elevation is used above the water level as follows

$$\phi_I(x, y, z, t) = \begin{cases} \frac{gA}{\omega}e^{kz}\sin(k(x + Ut)\cos\beta + ky\sin\beta - \omega t) & \text{for } z \le 0 \\ \frac{gA}{\omega}\sin(k(x + Ut)\cos\beta + ky\sin\beta - \omega t) & \text{for } 0 < z \le \zeta. \end{cases} \tag{14}$$

The nonlinear force can be obtained by direct integration of the hydrodynamic pressure induced by the incident waves on the exact wetted surface as follows:

$$\{F_{\text{F.K.}}\}_{\text{Non.}} = -\rho\iint_{S_B}\left\{\frac{\partial \phi_I}{\partial t} - \vec{U}\cdot\nabla\phi_I + \nabla\Phi\cdot\nabla\phi_I + \frac{1}{2}\nabla\phi_I\cdot\nabla\phi_I\right\}\vec{n}\,dS. \tag{15}$$

Similarly, the nonlinear restoring force is calculated by subtracting the linear hydrostatic force at the mean-body position from the force at the actual body position as follows:

$$\{F_{\text{Res.}}\}_{\text{Non.}} = \rho g\iint_{S_B}(-z)\vec{n}\,dS - \rho g\iint_{\overline{S}_B}(-z)\vec{n}\,dS. \tag{16}$$

The viscous damping force in roll motion should be modeled, because the amplitude of motion is sensitive to the viscosity of the fluid. The viscous force is generally proportional to quadratic of the roll angular velocity, but this study adopts an equivalent linear damping as suggested by Himeno (1981). Because the effects of variation of restoring force are more dominant in the occurrence and magnitude of parametric roll than those of damping forces, the computations are carried out based on a given linear damping force for an easier numerical implementation.

In this study, to model the viscous roll damping, a linear damping coefficient which is expressed as the ratio to the critical damping for roll motion is adopted.

$$b_{roll} = 2\gamma\sqrt{(M_{44} + A_{44,\infty})C_{44}} \tag{17}$$

where $A_{44,\infty}$ and C_{44} indicate the infinite-frequency added moment of inertia and the linear restoring coefficient in roll motion, respectively. The value of γ, which represents the ratio of damping force to the critical damping, can be determined by considering the decreasing tendency of roll amplitude in a free-roll-decay experiment. However, the ratio is varied depending on hull shape, ship speed, and appendages. In the present study, the values in the range of 0.03–0.10 which are appropriate for a typical hull are used to consider the effects of different roll damping forces.

2.3. Prediction of added resistance: weakly nonlinear near-field method

The added resistance of a ship is predicted by adopting the near-field method, namely, direct integration of second-order pressure on a body surface. The near-field method based on the linear displacement (linear-motion-based method) was derived by Joncquez (2009) and Kim and Kim (2011a) for the time-domain 3-D Rankine panel method. The second-order force can be formulated using the perturbation of physical and geometrical variables such as linear displacement, hydrodynamic pressure, wave elevation, and normal vector of the surface

Table 1
Classification of components in added resistance.

Total added resistance	$\vec{F_2} = (I) + (II) + (III) + (IV) + (V) + (VI) + (VII) + \{F_{\text{F.K.}}\}_{\text{H.O.T.}} + \{F_{\text{Res.}}\}_{\text{H.O.T.}}$	
Formulation	**Linear-motion-based method**	**Weakly nonlinear method**
Component (*I*)	$\frac{1}{2}\rho g\int_{WL}(\zeta-(\xi_3+\xi_4 y-\xi_5 x))^2\cdot\frac{\vec{n}}{\sin\alpha}dL$ $-\rho\int_{WL}\left(-\left(\vec{U}-\frac{1}{2}\nabla\Phi\right)\cdot\nabla\Phi\right)(\zeta-(\xi_3+\xi_4 y-\xi_5 x))\cdot\frac{\vec{n}_1}{\sin\alpha}dL$ $-\rho\int_{WL}\vec{\delta}\cdot\nabla\left(-\left(\vec{U}-\frac{1}{2}\nabla\Phi\right)\cdot\nabla\Phi\right)(\zeta-(\xi_3+\xi_4 y-\xi_5 x))\cdot\frac{\vec{n}}{\sin\alpha}dL$	$\frac{1}{2}\rho g\int_{WL}(\zeta-(\xi_3+\xi_4 y-\xi_5 x))^2\cdot\frac{\vec{n}}{\sin\alpha}dL$ $-\frac{1}{2}\rho g\int_{WL}(\zeta_I-(\xi_3+\xi_4 y-\xi_5 x))^2\frac{\vec{n}}{\sin\alpha}dL$ $-\rho\int_{WL}\left(-\left(\vec{U}-\frac{1}{2}\nabla\Phi\right)\cdot\nabla\Phi\right)(\zeta-(\xi_3+\xi_4 y-\xi_5 x))\cdot\frac{\vec{n}_1}{\sin\alpha}dL$ $-\rho\int_{WL}\vec{\delta}\cdot\nabla\left(-\left(\vec{U}-\frac{1}{2}\nabla\Phi\right)\cdot\nabla\Phi\right)(\zeta-(\xi_3+\xi_4 y-\xi_5 x))\cdot\frac{\vec{n}}{\sin\alpha}dL$
Component (*II*)	$-\rho\iint_{\bar{S}_B}gz\cdot\vec{n}_2 dS$	–
Component (*III*)	$-\rho\iint_{\bar{S}_B}\left(\frac{\partial(\phi_I+\phi_d)}{\partial t}-(\vec{U}-\nabla\Phi)\cdot\nabla(\phi_I+\phi_d)+g(\xi_3+\xi_4 y-\xi_5 x)\right)\cdot\vec{n}_1 dS$	$-\rho\iint_{\bar{S}_B}\left(\frac{\partial\phi_d}{\partial t}-(\vec{U}-\nabla\Phi)\cdot\nabla\phi_d\right)\cdot\vec{n}_1 dS$
Component (*IV*)	$-\rho\iint_{\bar{S}_B}\left(\frac{1}{2}\nabla(\phi_I+\phi_d)\cdot\nabla(\phi_I+\phi_d)\right)\cdot\vec{n}\,dS$	$-\rho\iint_{\bar{S}_B}\left(\nabla\phi_I\cdot\nabla\phi_d+\frac{1}{2}\nabla\phi_d\cdot\nabla\phi_d\right)\cdot\vec{n}\,dS$
Component (*V*)	$-\rho\iint_{\bar{S}_B}\vec{\delta}\cdot\nabla\left(\frac{\partial(\phi_I+\phi_d)}{\partial t}-(\vec{U}-\nabla\Phi)\cdot\nabla(\phi_I+\phi_d)\right)\cdot\vec{n}\,dS$	$-\rho\iint_{\bar{S}_B}\vec{\delta}\cdot\nabla\left(\frac{\partial\phi_d}{\partial t}-(\vec{U}-\nabla\Phi)\cdot\nabla\phi_d\right)\cdot\vec{n}\,dS$
Component (*VI*)	$-\rho\iint_{\bar{S}_B}\vec{\delta}\cdot\nabla\left(-\vec{U}\cdot\nabla\Phi+\frac{1}{2}\nabla\Phi\cdot\nabla\Phi\right)\cdot\vec{n}_1 dS$ $-\rho\iint_{\bar{S}_B}\left(-\vec{U}\cdot\nabla\Phi+\frac{1}{2}\nabla\Phi\cdot\nabla\Phi\right)\cdot\vec{n}_2 dS$	$-\rho\iint_{\bar{S}_B}\vec{\delta}\cdot\nabla\left(-\vec{U}\cdot\nabla\Phi+\frac{1}{2}\nabla\Phi\cdot\nabla\Phi\right)\cdot\vec{n}_1 dS$ $-\rho\iint_{\bar{S}_B}\left(-\vec{U}\cdot\nabla\Phi+\frac{1}{2}\nabla\Phi\cdot\nabla\Phi\right)\cdot\vec{n}_2 dS$
Component (*VII*)	$-\rho\iint_{\bar{S}_B}H\vec{x}\cdot\nabla\left(-\vec{U}\cdot\nabla\Phi+\frac{1}{2}\nabla\Phi\cdot\nabla\Phi+gz\right)\cdot\vec{n}\,dS$	$-\rho\iint_{\bar{S}_B}H\vec{x}\cdot\nabla\left(-\vec{U}\cdot\nabla\Phi+\frac{1}{2}\nabla\Phi\cdot\nabla\Phi\right)\cdot\vec{n}\,dS$
Higher-order Froude-Krylov force, $\{F_{\text{F.K.}}\}_{\text{H.O.T.}}$	–	$\{F_{\text{F.K.}}\}_{\text{Non.}}+\rho\iint_{\bar{S}_B}\left(\frac{\partial\phi_I}{\partial t}-(\vec{U}-\nabla\Phi)\cdot\nabla\phi_I\right)\cdot\vec{n}\,dS$
Higher-order restoring force, $\{F_{\text{Res.}}\}_{\text{H.O.T.}}$	–	$\{F_{\text{Res.}}\}_{\text{Non.}}+\rho\iint_{\bar{S}_B}gz\cdot\vec{n}_1\,dS+\rho\iint_{\bar{S}_B}g(\xi_3+\xi_4 y-\xi_5 x)\cdot\vec{n}\,dS$

with respect to the mean-body position. Therefore, the force contains only the quadratic components of the linear solutions. However, in the present weakly nonlinear prediction, the components of the added resistance induced by the Froude-Krylov and hydrostatic forces are replaced by the nonlinear forces at the actual surfaces of the body in waves. In other words, the higher-order forces are considered by subtracting the first-order forces from those in Eqs. (15) and (16). The added resistance denotes the mean value of the higher-order force in the longitudinal direction of a ship. Similar considerations for higher-order horizontal drifting effects on a ship in association with the incident wave can be found in Zhang et al. (2009).

For a physical observation, the added resistance is decomposed into nine integral terms as described in Table 1. Here, $\vec{n}_1$ and $\vec{n}_2$, are the first order and the second order normal vectors, respectively.

$$\vec{n}_1=\begin{bmatrix}0 & -\xi_6 & \xi_5\\ \xi_6 & 0 & -\xi_4\\ -\xi_5 & \xi_4 & 0\end{bmatrix}\begin{bmatrix}n_1\\ n_2\\ n_3\end{bmatrix} \tag{18}$$

$$\vec{n}_2=H\vec{n}=\frac{1}{2}\begin{bmatrix}-(\xi_5^2+\xi_6^2) & 0 & 0\\ 2\xi_4\xi_5 & -(\xi_4^2+\xi_6^2) & 0\\ 2\xi_4\xi_6 & 2\xi_5\xi_6 & -(\xi_4^2+\xi_5^2)\end{bmatrix}\begin{bmatrix}n_1\\ n_2\\ n_3\end{bmatrix}. \tag{19}$$

In addition, α in the waterline integral term, (*I*) indicates the inclination angle of hull geometry at the mean-water level as shown in Fig. 2. If the angle is 90°, the hull geometry is vertical wall-sided. Generally, for a typical ship model, the term, (*I*) is the main contributor to the second-order force. Therefore, the effect of the relative wave elevation on a body, which is the most important factor in the prediction of added resistance, is included through the value of α, considering the variation of hull geometry near the mean-water level. However, for large-amplitude ship motions, the nonlinear effects due to the geometry become stronger. In this circumstance, the integral term can be obtained more accurately by applying the higher-order Froude-Krylov and restoring forces, $\{F_{\text{F.K.}}\}_{\text{H.O.T.}}$ and $\{F_{\text{Res.}}\}_{\text{H.O.T.}}$ without solving a higher-order boundary value problem.

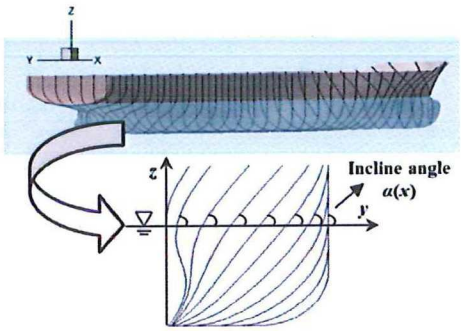

Fig. 2. Definition of inclination angle.

3. Analysis results

3.1. Ship model

The present numerical simulations are conducted on a 6500 TEU containership. The geometry of the ship has a large bow flare angle and an overhanging transom, which leads to the large variation in water plane area according to the relative position of the ship to the wave elevation as shown in Fig. 3. In the bow section, there is a small variation in the waterline, while the stern section shows a larger change because of the location of wave and body shape. This change results in the variation of the transverse stability, which is represented by the value of the GM. Therefore, it is known that this type of a ship is vulnerable to the parametric roll phenomena. The principle dimensions of the ship model are summarized in Table 2. All of the simulations are carried out in head sea (β = 180.0°) and at 5 knots forward-speed conditions.

In applications of the Rankine panel method, the discretized panels

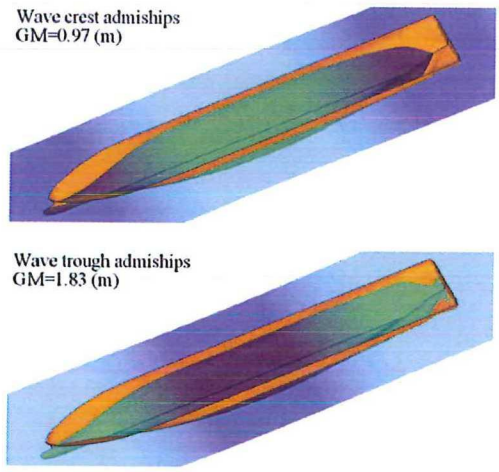

Fig. 3. Variation in water plane area and transverse stability: A/L = 0.005, λ/L = 1.0.

Table 2
Principle dimensions of 6500 TEU containership.

Designation	6500 TEU containership
LBP (m)	286.30
Beam (m)	40.30
Draft (m)	13.13 (AP), 12.97 (FP)
GM (m)	1.38
Natural period of roll (s)	30.21

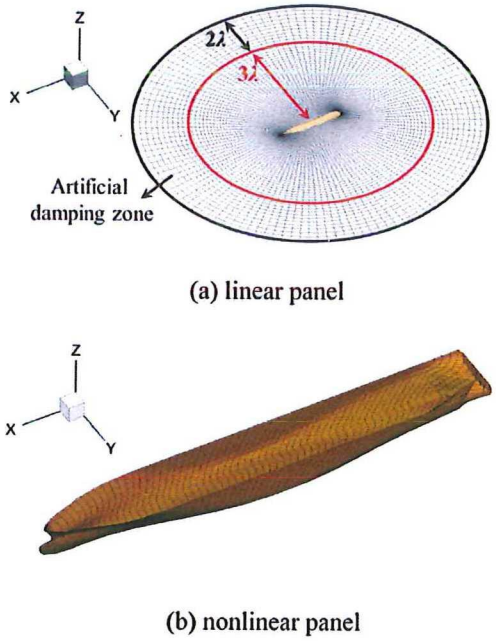

Fig. 4. Examples of solution grids.

are distributed on the body and the free surfaces. In case of the linear body panels, the grids are clustered near the fore and aft body, where the flow patterns are more complicated than those near the mid-ship. On the other hand, the number of the linear free surface panels varies according to the length of incident waves. The radius of the total domain is five times that of the wavelength, which consists of three wavelengths for the problem domain and two wavelengths for the artificial damping zone. In addition, the nonlinear body panels are modeled up to a certain height above the mean-water level to consider the nonlinear geometric effects at the exact wetted surfaces. Fig. 4 shows an example of the linear and nonlinear solution grids. For the grid convergence test, several grid systems of the linear panels are adopted as described in Table 3.

Table 3
Grid systems of linear panels in grid convergence test.

Grid number	Number of body panels	Number of free surface panels
Grid 1	750	1500
Grid 2	1500	1500
Grid 3	1500	2500
Grid 4	2500	2500
Grid 5	2500	4000
Grid 6	4000	4000

3.2. Motion response and added resistance in regular waves

Firstly, the responses of the vertical motions without the parametric roll are validated, because the motions are directly relevant to the added resistance, especially, the components depending on the relative wave elevation and the radiation. As there is no experimental data for the ship model, computation results of the present Rankine panel method are compared with those obtained by the Impulse response function (IRF) method. The present IRF method is based on the work of Fonseca and Soares (1998). In this method, hydrodynamic coefficients and wave excitation forces are computed by the two-dimensional strip theory (Salvesen et al., 1970), and then the frequency-domain solutions are converted to the time-domain solutions by convolution integral. The nonlinear Froude-Krylov and restoring forces are also considered according to the weakly nonlinear approach. The details of applications of the IRF method for the same simulation conditions can be found in Lee and Kim (2016).

From Fig. 5, it can be observed that there are good correlations between the amplitudes of the responses computed by the two different numerical methods. The phase angles of the responses that affect the relative wave elevation are also similar in the two methods. Furthermore, the weakly nonlinear motions are compared to the motion in the linear approach, where linear restoring coefficients and Froude-Krylov forces evaluated at the mean-body position are adopted. For relatively small wave amplitudes (A/L = 0.005–0.010), the weakly nonlinear and the linear motions show a good agreement as weak resonances of the vertical motions occur for the slow forward-speed (5 knots) condition. However, when the wavelength is similar to the length of the ship ($\omega(L/g)^{1/2} \approx 2.50$), discrepancies between the heave motions of the two approaches can be confirmed due to the large variation of the water plane area in the wave (Fig. 3). On the other hand, the variation is less effective on the phase angels of ship motions.

It is widely known that a second-order value is more sensitive to the grid system than a linear motion response. To obtain an accurate and a converged solution, the grid convergence test for added resistance on the ship model is carried out. Fig. 6 shows the computation results of the linear-motion-based method for the grid systems, which are present in Table 3. Over the grid system, which is composed of 2500 and 4000 panels on the mean-body surface and free surface, respectively (Grid 5), the convergent solutions can be seen for the different wavelengths. In addition, because the wave radiation is more dominant than the wave diffraction for a long wavelength, the added resistance is more stable along with the grid system than that for a short wavelength.

Next, the added resistances obtained by both the linear-motion-based method and the weakly nonlinear method are compared as shown in Fig. 7. The results of the weakly nonlinear method, which are not sensitive to the nonlinear panels are slightly different with those of the linear method at the peak of transfer function. There are two reasons for these discrepancies. First, the different heave motions of

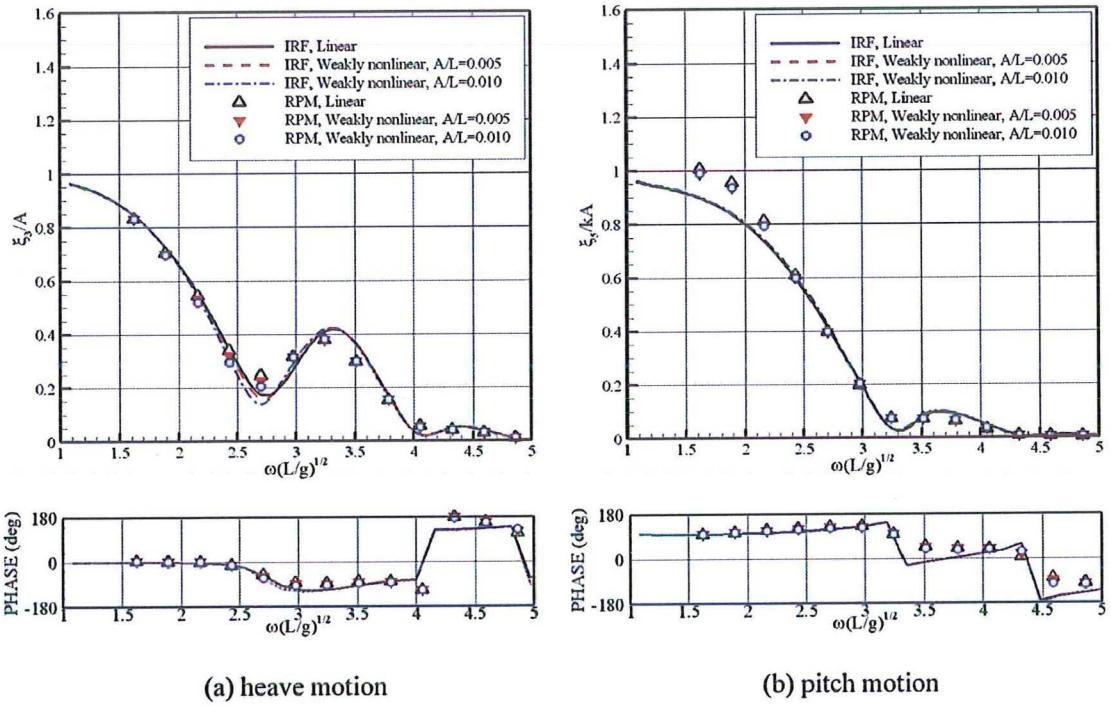

Fig. 5. Vertical motion responses.

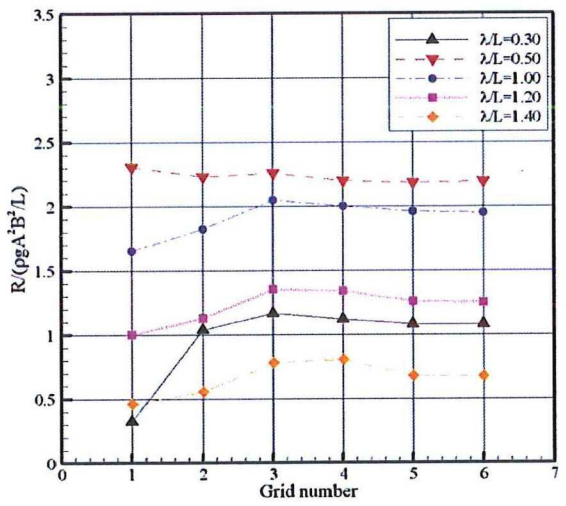

Fig. 6. Grid convergence test for added resistance.

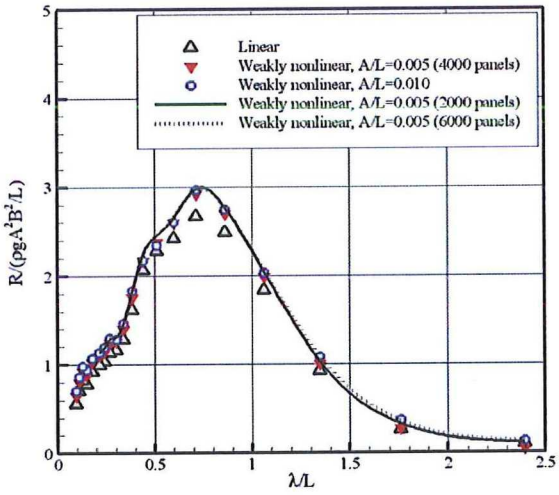

Fig. 7. Added resistance on ship: linear vs. weakly nonlinear methods.

the linear and nonlinear approaches change the components depending on the relative wave elevation and the radiation. Secondly, in the linear method, the nonlinear effects owing to body geometry are considered only using the inclination angle, (α), in the waterline integral term, while the weakly nonlinear method uses the forces evaluated at the exact wetted surface. Therefore, the term can be different for the wavelengths where larger variations of the water plane area occur. Except the peak region, the results of the two approaches are similar for small wave amplitudes, which indicate that the present weakly nonlinear method provides a consistent prediction compared to the linear method.

3.3. Added resistance in regular parametric roll motions

The simulation of the parametric roll for a regular wave is performed based on the present Rankine panel method along with the weakly nonlinear approach, and the results are compared with those of the IRF method. In both the numerical methods, an impulsive roll angle (3.0–10.0°) is imposed at an instant to model the initial disturbance of roll motion, which are induced by environmental conditions such as gusts or currents as shown in Fig. 8. After the initial condition, the regular parametric roll is excited resonantly by the variation of the transverse stability in the wave. Thereafter, the roll motion reaches a quasi-steady state as the development of motion is bounded by balancing the decreased variation of the nonlinear restoring force and the increased roll damping force at a large heel angel. Fig. 9 shows the quasi-steady-state amplitudes computed for conditions of different regular waves and damping forces. The wave conditions are chosen according to the vulnerable conditions to parametric roll phenomena; the wavelength is equivalent to the length of a ship, and the encounter wave frequency, ω_e is approximately twice that of natural roll frequency, ω_n and the wave amplitude is larger than

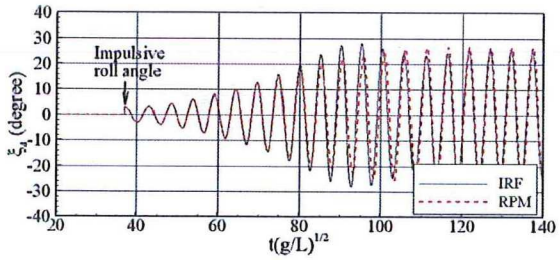

Fig. 8. Time histories of regular parametric roll: A/L = 0.005, λ/L = 1.35, γ = 0.03.

a certain threshold value. The two different numerical methods give similar overall trends for the occurrences and the magnitudes of the roll motions. The slight discrepancies may result from the different methods used for the calculation of the hydrodynamic forces; the 3-D boundary value problem is solved to obtain the force in the Rankine panel method, while the hydrodynamic coefficients calculated by the 2-D strip theory (Salvesen et al., 1970) are adopted in the IRF method. The natural roll frequency in a wave varies with the different added moment of inertia in roll motion, which leads to different predictions of the parametric roll because of the changed vulnerable condition related with the wave frequency.

In the present study, to investigate the effects of parametric roll on added resistance, the numerical simulations are performed with and without parametric roll for the same wave condition. For the case without parametric roll, the impulsive roll angle is not imposed during the simulation, and the both linear and weakly nonlinear approaches are adopted for the computations. On the other hand, in the simulation of parametric roll, the impulsive angle is imposed at a certain instant for the development of roll motion as shown in Fig. 8. Also, only the weakly nonlinear approach which can consider the variation of transverse stability in waves is applied for the simulation. If the parametric roll does not occur for a wave condition, the weakly nonlinear approach provides the same results regardless of the impulsive roll angle since the roll motion converges to zero from the initial condition due to damping forces.

For a vulnerable condition of parametric roll, the higher-order surge forces on the ship calculated using the linear-motion-based method and the weakly nonlinear method are compared as shown in Fig. 10. In the linear method, the sinusoidal solution, which is composed of the products of the linear physical and geometrical quantities of the encounter wave frequency, oscillates two times faster ($2\omega_e$) than the linear quantities when the parametric roll is not excited. On the other hand, slight modulations exist in the result of the weakly nonlinear method owing to the higher-order (over second-order) effects in the nonlinear restoring and Froude-Krylov forces. When the heavy parametric roll motion occurs, the behavior of the force is changed severely. The stronger nonlinear appearances can be seen, and the component of, ω_e, is dominant in that the roll motion oscillates with the natural roll frequency ($\omega_n \approx \omega_e/2$).

Fig. 11 shows the added resistance, that is, the temporal mean value of higher-order surge force. For the wave conditions where parametric roll does not occur, only the computation results without the phenomena are plotted. For the vulnerable conditions (A/L = 0.005, γ = 0.03, λ/L = 1.25–1.65; A/L = 0.010, γ = 0.10, λ/L = 1.05–1.75 as shown in Fig. 9), the added resistances increase significantly due to parametric roll motions compared to those in the absence of the phenomena. The effects of the nonlinear restoring and Froude-Krlyov forces at the exact wetted surfaces for large roll motions are accounted in the increments of added resistances based on the weakly nonlinear approach. It should be noted that the increased added resistance is not directly relevant to the wave amplitude, because the real values of the increments are similar for different regular wave conditions. However, the steady-state amplitudes of the roll motions are similar for the two conditions due to the different roll damping forces. Therefore, the increased resistance induced by the parametric roll seems to be closely related with the magnitude of the resulting roll motion.

For a physical observation, each component of the added resistance in the weakly nonlinear method described in Table 1 is investigated as shown in Fig. 12. The components with or without parametric roll are compared to determine the component that contributes to the increased resistance. When the roll motion is not excited, it can be seen that the waterline integral term, (*I*), and the higher-order Froude-Krylov force, which depend on the relative wave elevation, are dominant. In addition, the radiation components, such as (*III*) and (*V*) as observed in Table 1, have significant influences for relatively long wavelengths ($\lambda/L \approx$ 1.0–2.0). These components vary significantly owing to the parametric roll, and still remain the main terms in the added resistance. The largest component is the Froude-Krylov force evaluated at the actual wetted surface considering heavy roll motion. It should be noted that the term depending on the kinetic energy of the fluid, (*IV*), becomes the second contributor to the resistance; however, this term is not significant if the parametric roll does not occur.

The present results of the increased added resistance cannot be validated as there are no experimental data and other computation

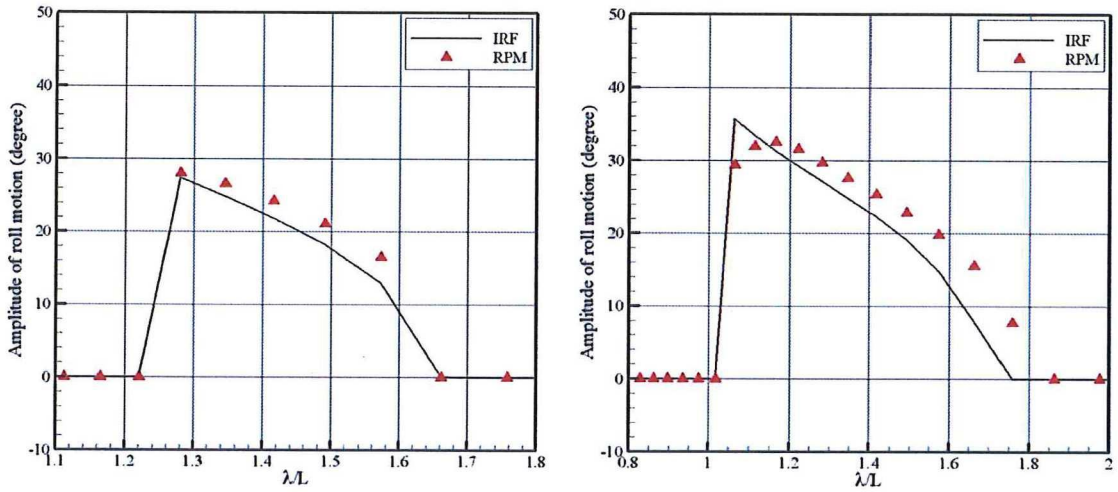

Fig. 9. Quasi-steady-state amplitude of regular parametric roll.

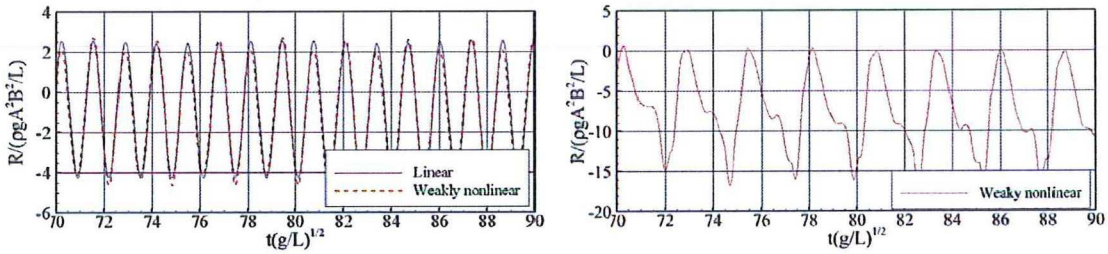

Fig. 10. Time histories of higher-order surge force: A/L = 0.005, λ/L = 1.35, γ = 0.03.

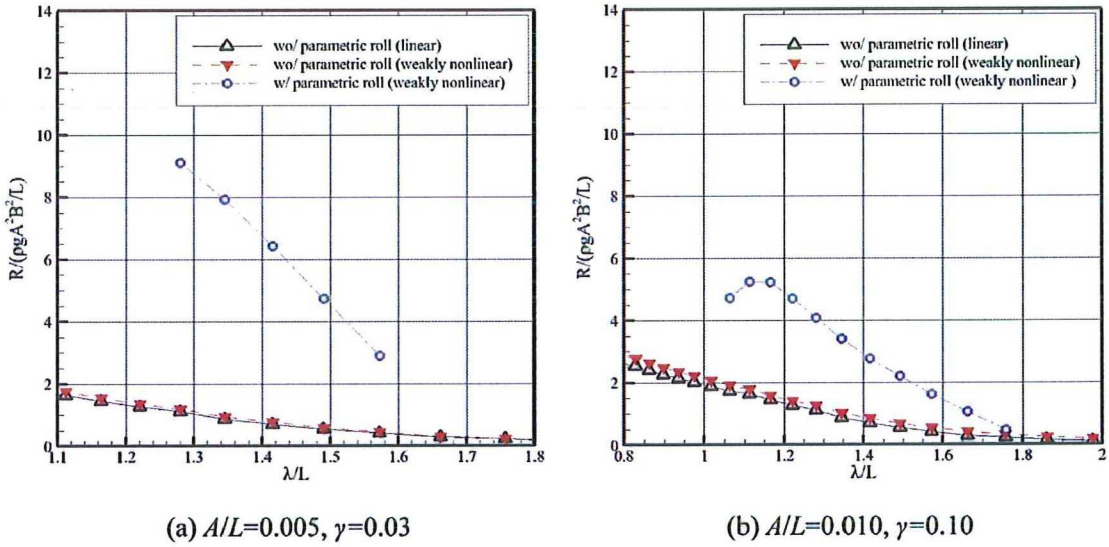

Fig. 11. Added resistance on ship in regular parametric roll.

results. It is merely confirmed that the experimental data of Lu et al. (2015) for a similar ship model shows similar tendencies with the results of this study; the increment in the resistance is 3 or 4 times under parametric roll motions of approximately 30°. As the main components, such as (*I*), (*III*), (*IV*), and (*V*), are dependent on the elevation or the velocity potential of the disturbed wave, strict considerations for the disturbance should be carried out to obtain an enhanced solution. As shown in Fig. 13, asymmetric and significantly severe disturbed waves are generated near the ship; especially in the bow region because of the excitation of the parametric roll. In the present study, the linear potential and the elevation are calculated with respect to the mean-body position; hence, there is a limitation to include the nonlinearities in the disturbance induced by the large-amplitude motion. Therefore, an application of fully nonlinear computation, for example, the CFD method may be required for more accurate prediction of the terms related with the nonlinear disturbance.

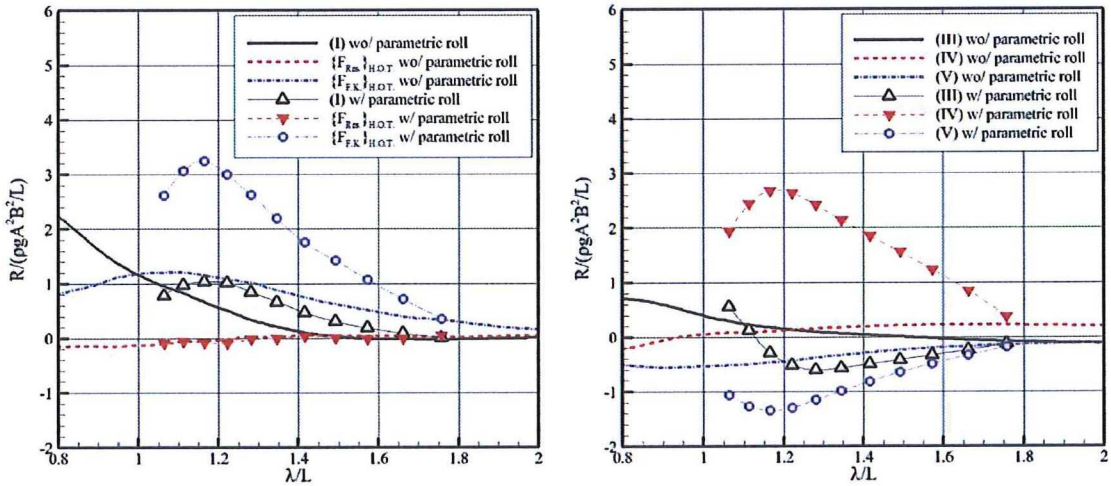

Fig. 12. Components of added resistance: A/L = 0.010, γ = 0.10.

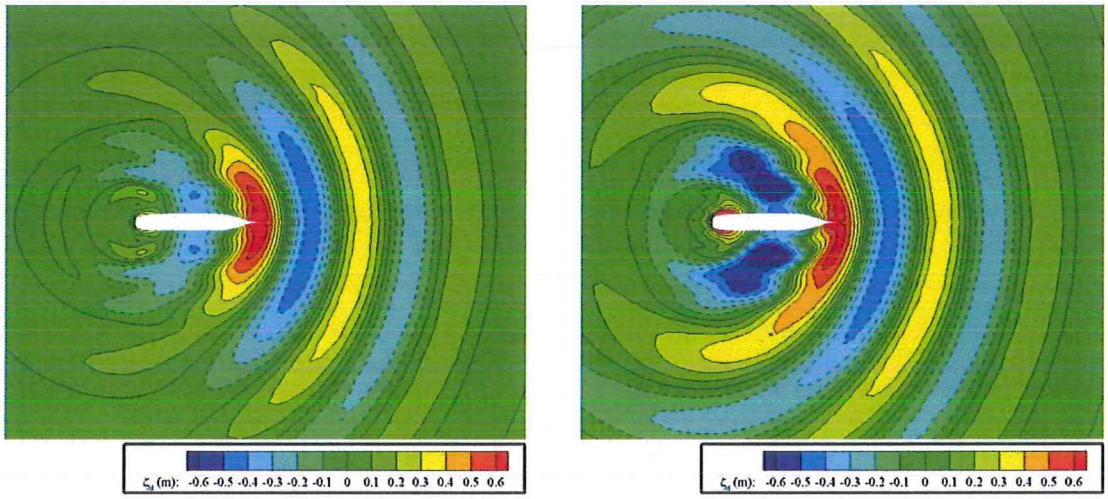

(a) without parametric roll (b) with parametric roll

Fig. 13. Disturbed wave contours around ship: A/L = 0.010, λ/L = 1.35, γ = 0.10.

3.4. Correlation between parametric roll and added resistance

Under the assumption that the higher-order quantities in the present weakly nonlinear approach are negligible, the added resistance can be regarded as a mean value of quadratic components of linear variables. The products of the quantities of the vertical motions (oscillating with ω_e) and the roll motion (oscillating with $\omega_n \approx \omega_e/2$) are represented by the components with frequencies of $\omega_e/2$ (difference-frequency) and $3\omega_e/2$ (sum-frequency) without a mean value. Evidently, the wave excitation force on the heave and pitch motions may contain the component of the natural roll frequency due to a nonlinear coupling in large roll motion. However, the radiation is more dominant than the diffraction for longer wavelengths; hence the nonlinear effects are also negligible. As a result, the increased resistance ($R_{w/PR} - R_{wo/PR}$) is considered to depend only on the resulting parametric roll. In this study, the second-order value is assumed to be proportional to the square of the amplitude of the roll angle according to the decoupling phenomena based on a linear perspective. As shown in Fig. 14, the correlation can be valid when the amplitude is smaller than 30°. Above this angle, the correlation is changed owing to stronger nonlinear effects such as the weakly nonlinear coupling of the vertical and roll motions and the higher-order (over second-order) restoring and Froude-Krylov forces.

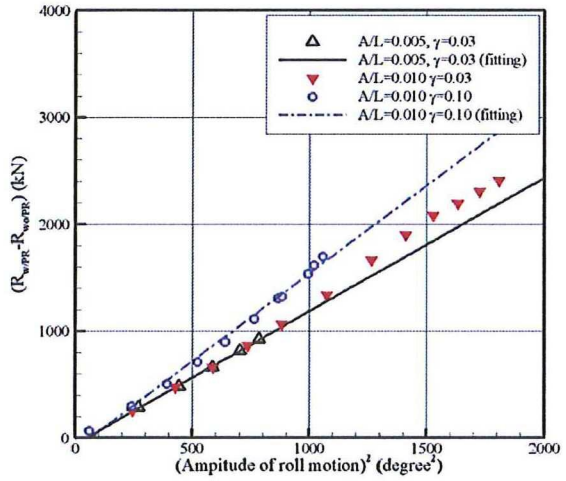

Fig. 14. Correlation between parametric roll and increased added resistance.

Furthermore, the relationship is slightly different according to the magnitude of the roll damping force, which can affect the period and amplitude of the parametric roll. In the present study, the viscous damping force is modeled by a linear damping. Therefore, the effects of nonlinear damping force on the parametric roll and the resulting added resistance should be thoroughly examined in the future. By adding nonlinear velocity components to the linear damping, the present methodology can be applied for the examination, and will also provide a solution of improved accuracy.

3.5. Weakly nonlinear coupling phenomena

In the weakly nonlinear analysis, the nonlinear coupling between the restoring forces of vertical motions and roll motion is accounted, and the variations of roll restoring moments due to waves and vertical motions lead to the parametric roll phenomena. When the amplitude of roll motion is not large, the effects of roll motion on vertical motions can be regarded negligible. Under heavy roll motions, however, there exist nonlinear coupling effects of the parametric roll on the vertical motions since the actual wetted surface varies significantly according to the roll motions, which affect the stiffness for the vertical motions. Lu et al. (2013) investigated the effects by conducting a free-running experiment and a numerical simulation based on the 3-DOF coupling mathematical model. Fig. 15 shows the time histories of motions of ship under parametric roll. The vertical motions are changed severely according to occurrence of the phenomena when the amplitude of roll motion is above 30°. Especially, the heave motion varies more greatly compared to the pitch motion, and the strong nonlinear behaviors, such as subharmonic components, are confirmed. As shown in Fig. 16, not only the amplitudes, but also the mean values of vertical motions are changed due to the restoring coupling. These tendencies become intensified as the amplitude of the roll angle increases.

The changed vertical motions again affect the parametric roll and the resulting added resistances. First, the natural roll frequency and the variation of transverse stability in waves are changed due to the resulting mean values (steady posture of ship in waves) and amplitudes, respectively. These variations have parametric roll less divergent even for a large wave amplitude (detuning phenomena) since the ship gets out of the vulnerable conditions related with the natural roll frequency ($\omega_n \approx \omega_e/2$). Spanos and Papanikolaou (2009) confirmed the decay of parametric resonance for higher wave steepness, and the

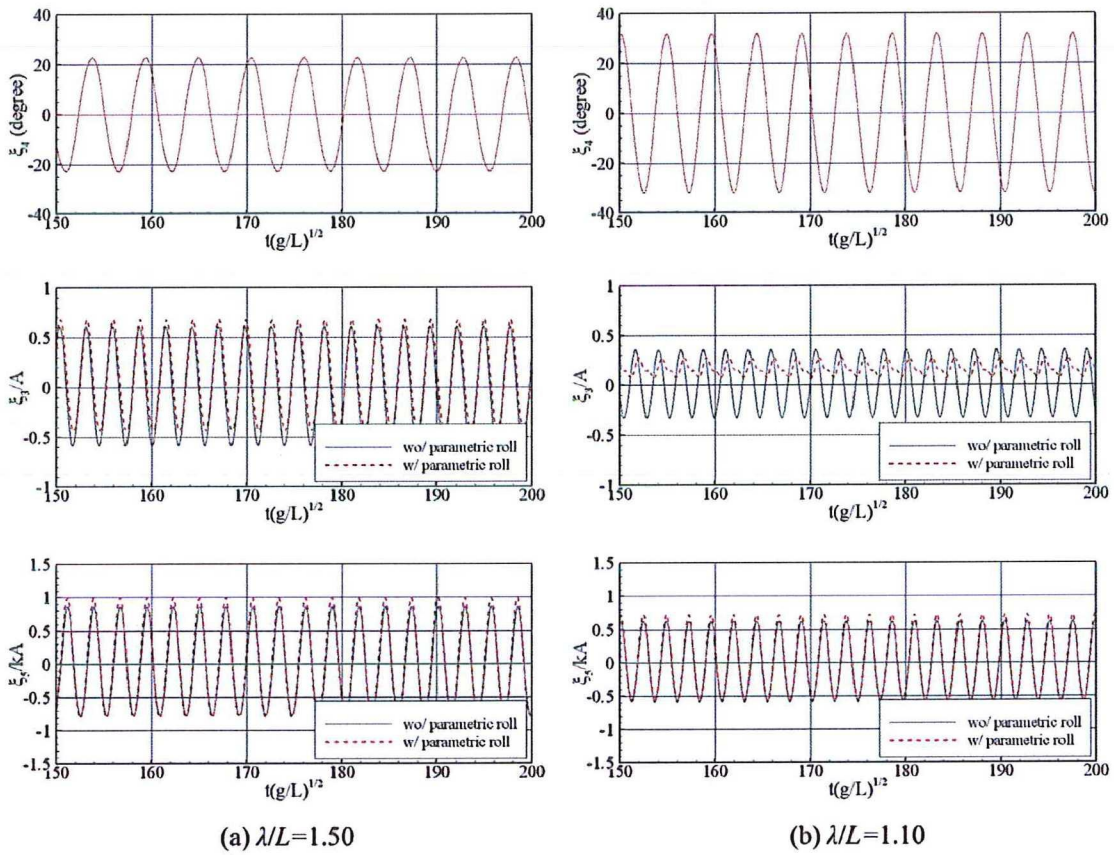

Fig. 15. Time histories of ship motions: A/L = 0.010, γ = 0.10, parametric roll (top), heave motion (middle), pitch motion (bottom).

detuning effects may be one of the causes of the decaying tendency. Secondly, the component of added resistance induced by roll motion can be varied since the component depends on the resulting amplitude of parametric roll. Also, the components induced by vertical motions are affected by the changed relative wave elevation and the radiation. The key assumption for the derived correlation between the parametric roll and the increased resistance is the decoupling phenomena, in which the resistance of the vertical motions remains constant with or without the roll motion. Therefore, the changed vertical motions are the main reasons for violating the relationship in large roll motions. This trend can be evaluated more accurately based on the weakly nonlinear approach than the linear-motion-based method; therefore, the correlation according to a linear perspective is not appropriate when severe roll motion arises.

3.6. Added resistance in irregular parametric roll motions

To generate irregular waves, the JONSWAP spectrum with a peak

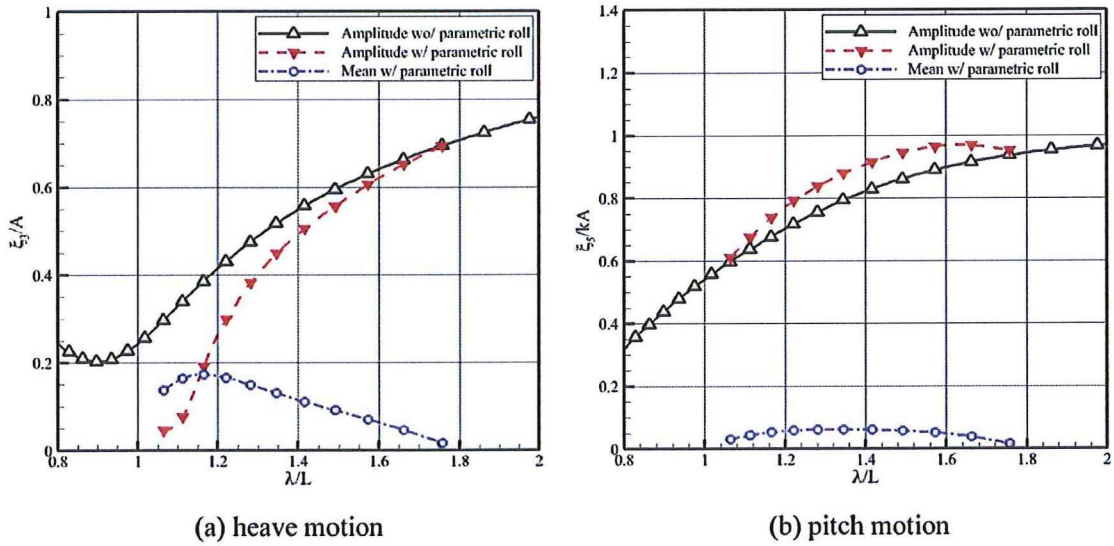

Fig. 16. Vertical motion responses: A/L = 0.010, γ = 0.10.

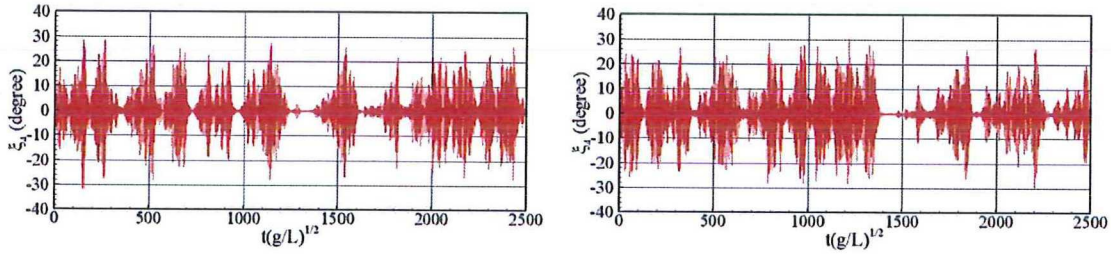

Fig. 17. Time histories of irregular parametric roll.

enhancement factor, γ_{peak} of 3.3 is adopted, and the spectrum is discretized by randomly distributed 100 wave components. The significant wave height, *Hs* and the modal period, *Tp* are set to 5.25 m and 16.5 s, respectively, in which the frequency at the peak of spectrum corresponds to the vulnerable condition related with wave frequency ($\omega_n \approx \omega_e/2$). Fig. 17 shows the time histories of irregular parametric roll motions computed using the present method. The time variable, t is normalized by the gravitational acceleration and the length of ship as follows; $t(g/L)^{1/2}$. The amplitudes of the roll motions are continuously time-varying without attaining any quasi-steady states. In addition, for the different sets of phases of wave components (different realizations), relatively different behaviors of roll motions can be seen. In irregular waves, the simulation results of the parametric roll present strong uncertainties and sensitivities to computation parameters, such as the length of the time window and the discretized wave components, owing to the non-Gaussianities and non-ergodicities in the nonlinear system. For various conditions for the parameters, Park et al. (2013) examined the sensitivities by conducting the time-domain simulations based on the IRF method. As previously mentioned, the increased added resistance in parametric roll depends on the amplitude of roll motion. Therefore, to evaluate the resistance, a stochastic analysis through various realizations should be conducted in consideration of the uncertainties in the prediction of the parametric roll.

In this study, a simple prediction method for the added resistance in irregular parametric roll motions is suggested according to the correlation derived from the regular computations. By neglecting the nonlinear effects, the total added resistance, R_{Total} can be resolved into the resistances of the vertical motions, R_{VM} and the parametric roll, R_{PR} based on the decoupling phenomena as follows

$$R_{Total}(Hs, Tp, \bar{\xi}_4) = R_{VM}(Hs, Tp) + R_{PR}(\bar{\xi}_4) = 2\int_0^\infty R(\omega)S_\zeta(\omega)d\omega + k\bar{\xi}_4^2 \tag{20}$$

where $R(\omega)$ and $S_\zeta(\omega)$ indicate the normalized added resistance of the vertical motions with respect to the square of the wave amplitude and the wave spectrum, respectively. The R_{VM} is calculated by the summation of the added resistance of each wave component. In addition, the value of k is a coefficient determined by curve fitting the increased added resistance and the square of amplitude of roll, $\bar{\xi}_4^2$ as shown in Fig. 14. Fig. 18 shows the time histories of the higher-order surge forces with or without parametric roll for realization 1. The distributions of the peak values are similar regardless of the occurrence of the phenomena while the mean value seems to be changed due to the roll motions. According to the time-varying amplitude of roll motion, the mean also varies as the simulation progresses. Therefore, to investigate the time-varying added resistance, the interval mean, which denotes the mean value for ten periods of roll motion (approximately 60.0 in normalized time) near a certain instant, is plotted as shown in Fig. 19. When the parametric roll is not excited, it can be seen that the interval mean is similar to the R_{VM}. The discrepancies between the two values result from the short length of the time window. On the other hand, the temporal mean, which is the mean for the total previous time history, converges to the R_{VM} in a transient period of ~ 500.0 in normalized time. The analysis on the sensitivities of the added resistance on the length of the time window and the wave components can be found in the study by Kim and Kim (2011a). During parametric roll, the interval mean oscillates according to the development of the parametric roll. It can be seen that this time-varying mean is bounded by the calculated value of Eq. (20) for the corresponding roll angle, which indicate that the correlation between the increased added resistance and the parametric roll can be valid under 30° of roll motions. In conclusion, without time-consuming irregular computations, the total added resistance can be easily predicted by this method if the distribution of irregular parametric roll is known by an efficient method such as the semi-analytic method of Lee and Kim (2016).

4. Conclusions

The added resistance on a containership in regular and irregular parametric roll is investigated by applying the time-domain 3-D Rankine panel method. To consider the large-amplitude roll motion, a weakly nonlinear approach for the prediction of the added resistance is adopted. From this study, the following conclusions can be drawn:

- The present weakly nonlinear approach provides a consistent result compared with that of the linear-motion-based method for relatively smaller wave amplitudes. When the wavelength is similar with the

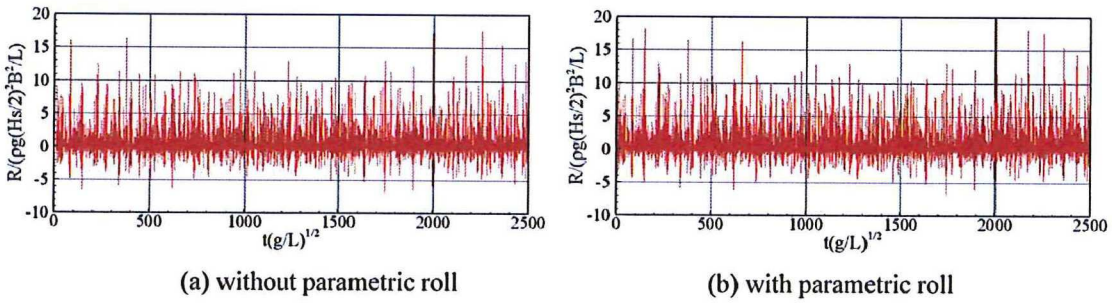

Fig. 18. Time histories of higher-order surge force: realization 1.

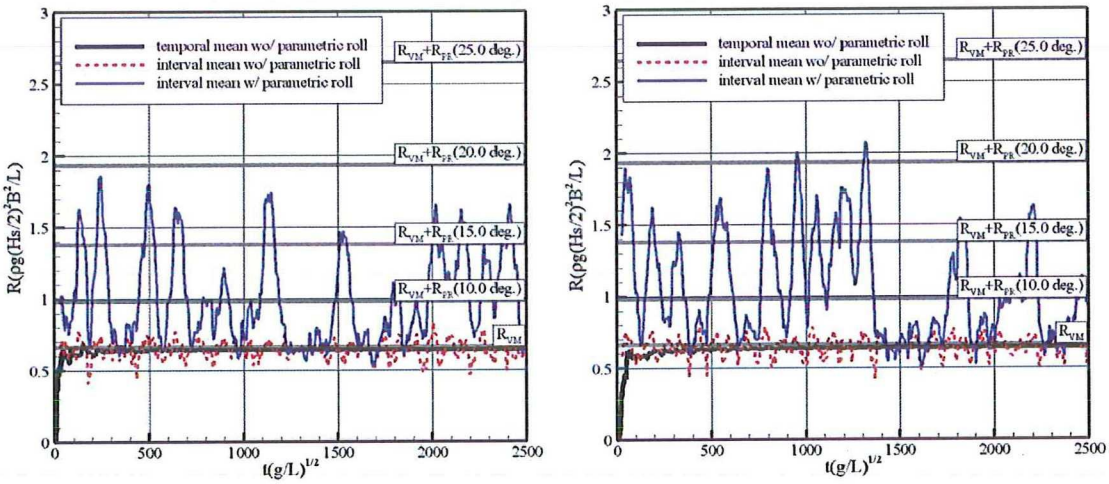

Fig. 19. Time histories of added resistance in irregular parametric roll.

length of ship, slight discrepancies arise, which indicates that the inclination angle in the linear method has a limitation in considering the large variation of wetted surface in a wave for the present ship model.

- A significant increase in the added resistance induced by the parametric roll motion is confirmed. The effects of the nonlinear restoring and Froude-Krlyov forces at the exact wetted surfaces for large roll motions are accounted in the increment of added resistance based on the weakly nonlinear approach. Through the decomposition analysis, it is found that the higher-order Froude-Krylov force and the component related with the kinetic energy of the fluid are the main contributors for the increased resistance.
- The correlation for the increased added resistance and the parametric roll is derived according to the decoupling phenomena between the vertical motions and the roll motion based on a linear perspective. The relationship is verified by curve fitting the increment and the square of the amplitude of the roll angle. For a larger roll motion of above 30°, the correlation can be changed owing to the nonlinear coupling effects and the contributions of more higher-order components. In addition, it is seen that the damping force in roll motion can affect the relationship by changing the period and amplitude of the parametric roll.
- It is seen that the weakly nonlinear coupling effects become intensified as the amplitude of the roll motion increases. The changed mean values and amplitudes of vertical motions can affect the variation of the wetted surface, which should be included in the prediction of the parametric roll. Furthermore, the vertical motions change the component of the added resistance depending on the relative wave elevation and the radiation, which implies that the derived correlation is not valid for larger roll motions.
- Based on the correlation, a simple prediction method for the added resistance in irregular parametric roll is suggested. By comparing with the time-varying added resistance obtained by direct time-domain simulation, it can be shown that the method can give the boundary value of the added resistance for the corresponding roll angle without time-consuming irregular computations.

Acknowledgement

This study was partly funded by the Ministry of Trade, Industry and Energy (MOTIE), Korea, under Industrial Technology Innovation Program, No. 10062881, "Technology Development to Improve Added Resistance and Ship Operational Efficiency for Hull Form Design," and the Lloyd's Register Foundation (LRF)-Funded Research Center at Seoul National University, (No. G/0043). Moreover, RIMSE and AMEC of SNU are credited for their administrative support.

References

Breu, D., Fossen, T.I., 2010. Extreme seeking speed and heading control applied to parametric roll resonance. IFAC Proc. Vol. 43 (20), 28–33.

Faltinsen, O.M., Minsaas, K.J., Liapis, N., Skjørdal, S.O., 1980. Prediction of resistance and propulsion of a ship in a seaway. In: Proceedings of the 13th Symposium on Naval Hydrodynamics. Tokyo, Japan, pp. 505–529.

Fonseca, N., Soares, C.G., 1998. Time-domain analysis of large-amplitude vertical ship motions and wave loads. J. Ship Res. 42 (2), 139–153.

France, W.N., Levadou, M., Treakle, T.W., Paulling, J.R., Michel, R.K., Moore, C., 2003. An investigation of head-sea parametric rolling and its influence on container lashing systems. Mar. Technol. 40 (1), 1–19.

Fujii, H., Takahashi, T., 1975. Experimental study on the resistance increase of a ship in regular oblique waves. In: Proceedings of the 14th ITTC. Ottawa, Canada, pp. 351–360.

Gerritsma, J., Beukelman, W., 1972. Analysis of the resistance increase in waves of a fast cargo ship. Int. Shipbuild. Prog. 19, 285–293.

Grue, J., Biberg, D., 1993. Wave forces on marine structures with small speed in water of restricted depth. Appl. Ocean Res. 15, 121–135.

Himeno, Y., 1981. Prediction of Ship Roll Damping-state Of The Art. Report of NA & ME, 239 239. University of Michigan, AnnArbor, Michigan, USA.

Holden, C., 2011. Modeling and Control of Parametric Roll Resonance (Ph.D. Thesis). Norwegian University of Science and Technology, Trondheim, Norway.

Jensen, J.J., Beck, R.F., Du, S., Faltinsen, O.M., Fonseca, N., Rizzuto, E., Stredulinsky, D., Watanabe, I., 2000. Extreme hull girder loading. In: Proceedings of the 14th International Ship and Offshore Structures Congress. Elsevier Science, New York, USA, vol. 2, pp. 263–320.

Joncquez, S.A.G., 2009. Second-Order Forces and Moments Acting on Ships in Waves (Ph.D. Thesis). Technical University of Denmark, Copenhagen, Denmark.

Journee, J.M.J., 1992. Experiments and Calculations on 4 Wigley Hull Forms in Head Waves. Report 0909. Delft University of Technology, Delft, Netherlands.

Kim, K.H., Kim, Y., 2011a. Numerical study on added resistance of ships by using a time-domain Rankine panel method. Ocean Eng. 38, 1357–1367.

Kim, T.Y., Kim, Y., 2011b. Multi-level approach for parametric roll analysis. Int. J. Nav. Archit. Ocean Eng. 3 (1), 53–64.

Kim, Y., Kim, K.H., Kim, J.H., Kim, T.Y., Seo, M.G., Kim, Y., 2011. Time-domain analysis of nonlinear motion responses and structural loads on ships and offshore structures: development of WISH Programs. Int. J. Nav. Archit. Ocean Eng. 3 (1), 37–52.

Lee, J.H., Kim, Y., 2016. Development of a semi-analytical method for the efficient prediction of parametric roll. Ocean Eng. 112, 1–15.

Levadou, M., van't Veer, R., 2011. Parametric Roll and Ship Design. Contemporary Ideas on Ship Stability and Capsizing in Waves. Springer, Netherlands, 307–330.

Lu, J., Gu, M., Umeda, N., 2013. A study on the effect of parametric rolling on heave and pitch motions in head seas. In: Proceedings of the 13th International Ship Stability Workshop. Brest, France, pp. 185–191.

Lu, J., Gu, M., Umeda, N., 2015. A study on the effect of parametric rolling on added resistance in regular head seas. In: Proceedings of the 12th International Conference on the Stability of Ships and Ocean Vehicles. Glasgow, UK, vol. 2, pp. 681–688.

Maruo, H., 1960. The drift of a body floating on waves. J. Ship Res. 4, 1–10.

Newman, J.N., 1967. The drift force and moment on ships in waves. J. Ship Res. 11,

51–60.
Orihara, H., Miyata, H., 2003. Evaluation of added resistance in regular incident waves by computational fluid dynamics motion simulation using an overlapping grid system. J. Mar. Sci. Technol. 8, 47–60.
Orihara, H., Matsumoto, K., Yamasaki, K., Takagishi, K., 2008. CFD simulations for development of high-performance hull forms in a seaway. In: Proceedings of the 6th Osaka Colloquium on Seakeeping and Stability of Ship. Osaka, Japan, pp. 58–65.
Park, D.M., Kim, Y., Song, K.H., 2013. Sensitivity in numerical analysis of parametric roll. Ocean Eng. 67, 1–12.
Salvesen, N., Tuck, E.O., Faltinsen, O.M., 1970. Ship motions and sea loads. Trans.-Soc. Nav. Archit. Mar. Eng. 78, 250–279.
Shin, Y.S., Belenky, V.L., Weems, K.M., Lin, W.M, 2004. Criteria for parametric roll of large containerships in longitudinal seas. Trans.-Soc. Nav. Archit. Mar. Eng. 112, 14–47.
Song, K.H., Kim, Y., Park, D.M., 2013. Quantitative and qualitative analyses of parametric roll for ship design and operational guidance. Proc. Inst. Mech. Eng. Part M: J. Eng. Marit. Environ. 227 (2), 177–189.
Spanos, D., Papanikolaou, A., 2007. Numerical simulation of parametric roll in head seas. Int. Shipbuild. Prog. 54 (4), 249–267.
Spanos, D., Papanikolaou, A., 2009. On the decay and disappearance of parametric roll of ships in steep head waves. In: Proceedings of the 10th International Conference on the Stability of Ships and Ocean Vehicles. St. Petersburg, Russia, pp. 559-566.
Vidic-Perunovic, J., Jensen, J.J., 2009. Parametric roll due to hull instantaneous volumetric changes and speed variations. Ocean Eng. 36 (12), 891–899.
Yang, K.K., 2015. Analysis of Added Resistance on Ships in Waves Based on Cartesian-Grid Method (Ph.D. Thesis). Seoul National University, Seoul, Korea.
Zhang, S., Weems, K.M., Lin, W.M., 2009. Investigation of the horizontal drifting effects on ships with forward speed. In: Proceedings of the ASME 2009 28th International Conference on Ocean, Offshore, and Artic Engineering. Honolulu, Hawaii, USA.